FLAP-LAG-TORSION STABILITY IN FORWARD FLIGHT

Brahmananda Panda
Graduate Student
and
Inderjit Chopra
Associate Professor

Center for Rotorcraft Education and Research
Department of Aerospace Engineering
University of Maryland
College Park, MD 20742

ABSTRACT

An aeroelastic stability of three-degree flap-lag-torsion blade in forward flight is examined. Quasisteady aerodynamics with a dynamic inflow model is used. The nonlinear time dependent periodic blade response is calculated using an iterative procedure based on Floquet theory. The periodic perturbation equations are solved for stability using Floquet transition matrix theory as well as constant coefficient approximation in the fixed reference frame. Results are presented for both stiff-inplane and soft-inplane blade configurations. The effects of several parameters on blade stability are examined, including structural coupling, pitch-flap and pitch-lag coupling, torsion stiffness, steady inflow distribution, dynamic inflow, blade response solution and constant coefficient approximation.

NOTATIONS

a	= lift curve slope
$\underset{\sim}{A}$	= matrix in first order equations in rotating system
$\underset{\sim}{A}_f$	= matrix in first order equations in fixed system
$\underset{\sim}{B}_1, \underset{\sim}{B}_2$	= matrices in dynamic inflow equations
c	= blade chord
C_d	= blade section drag coefficient
C_ℓ	= blade section lift coefficient
C_m	= blade section moment coefficient
$\underset{\sim}{C}_r, \underset{\sim}{C}_r^p$	= damping matrices in response and perturbed equations respectively
C_T	= thrust coefficient, $T/\pi\rho\Omega^2R^4$
C_w	= weight coefficient, $W/\pi\rho\Omega^2R^4$
$C_{d_\alpha}, C_{\ell_\alpha}, C_{m_\alpha}$	= differential aerodynamic coefficients wrt α
D	= drag force of the helicopter
e	= hinge offset divided by rotor radius
f	= equivalent drag area of helicopter
$\underset{\sim}{F}_{NL}$	= nonlinear force vector in response equation
I_b	= moment Inertial of blade (flap)
I_f^*	= ratio of torsional inertia to blade flap inertia
h	= distance of hub from helicopter c.g.
H	= rotor drag force, positive rearward
K_{p_β}, K_{p_ζ}	= pitch-flap and pitch-lag couplings respectively
$\underset{\sim}{K}_r, \underset{\sim}{K}_r^p$	= stiffness matrices in response and stabilty equations
K_x, K_y	= coefficients in Drees model
$\underset{\sim}{\ell}, \underset{\sim}{m}$	= coefficient matrices in dynamic inflow equation
$\underset{\sim}{M}_r, \underset{\sim}{M}_r^p$	= mass matrices in response and stability equations
M_{xf}, M_{yf}	= Aerodynamic rolling and pitching moments respectively
$M_\beta, M_\zeta, M_\theta$	= aerodynamic flap, lag and pitch moments respectively
N_b	= number of blades
$\underset{\sim}{N}_f$	= matrix in fixed system defined by eqn. (29)
$\underset{\sim}{Q}$	= transition matrix
R	= rotor radius
R_s	= structural coupling parameter

Presented at the Second Decennial Specialists' Meeting on Rotorcraft Dynamics at Ames Research Center, Moffett Field, CA, November 7-9, 1984.

T	=	rotor thrust force
U_p, U_t	=	blade section normal and inplane velocity
V	=	blade section resultant velocity, $\sqrt{U_t^2 + U_p^2}$
$\bar{V}$	=	forward speed
W	=	helicopter gross weight
x	=	blade radial coordinate (nondimensionalized wrt radius)
X_A	=	chordwise offset of blade aerodynamic center behind pitch axis
X_I	=	chordwise offset of blade center of gravity behind pitch axis
X_r	=	vector consisting degrees of freedom in rotating system
Y_r	=	state vector in rotating system
Y	=	rotor side force, positive towards advancing side
Y_f	=	fuselage side force
α	=	blade section angle of attack
α_k	=	real part of kth characteristic exponent
β,ζ,θ	=	angular deflections (flap, lag, torsion)
β_p	=	precone angle
γ	=	blade lock number, $\rho acR^4/I_b$
$\theta_0,\theta_{1c},\theta_{1s}$	=	collective, lateral cyclic, longitudinal cyclic pitch angles
λ	=	rotor inflow ratio
λ_k	=	kth characteristic exponent
μ	=	advance ratio, $V \cos\alpha/\Omega R$
$\nu_\beta,\nu_\zeta,\nu_\theta$	=	rotating flap, lag and torsional frequencies
ω_β, ω_ζ, ω_θ	=	nonrotating flap, lag and torsional frequencies
ρ	=	air density
σ	=	solidity ratio, $N_b c/\pi R$
ϕ	=	section induced angle, $\tan^{-1} U_p/U_t$
ϕ_s	=	lateral tilt of shaft
ψ	=	azimuth angle of the blade
ω_k	=	imaginary part of the kth exponent
Ω	=	speed of rotation
$\delta()$	=	perturbation quantity

INTRODUCTION

Several researchers have examined the aeroelastic stability of a helicopter blade in hover and forward flight (see recent reviews [1-3]). The phenomenon is complex involving nonlinear structural, inertial and aerodynamic forces. With a forward flight, the equations of blade motion get more involved because of the presence of many periodic terms. Due to the complexities of formulation and analysis of rotorary-wing dynamics problems, most of the analytical studies are of limited scope; more so, in forward flight conditions. The objective of the present paper is to examine aeroelastic stability in forward flight, including the effects of dynamic inflow on stability results. For this a simple flap-lag-torsion blade model consisting of three degrees of motion will be studied.

For design and analysis of a helicopter rotor, it is essential to analyze its aeroelastic stability. For this, a study on the dynamics of a single blade forms an important fundamental step to the complete understanding of the rotor-body dynamics. The blade stability analysis consists of three major phases; vehicle trim, blade steady response and stability of perturbation motion. The vehicle trim solution determines control settings for perscribed flight conditions and is calculated from the vehicle overall equilibrium equations. The blade response solution consists of time dependent blade position and is calculated from the blade equilibrium equations. In the calculations of blade response one needs the vehicle trim solution. For stability solution, a perturbation is given to the blade at its equilibrium position and the subsequent response amplitude is investigated for stability. For stability calculations, one needs the vehicle trim solution as well as blade response solution. These three phases of study are inherently coupled. A complete coupled solution is very involved and therefore most of the researchers uncouple these three phases and study each phase separately. It is possible however to achieve a certain degree of coupling between three phases through an iterative process.

The simplest form of a rotor blade representation is the rigid blade model with spring restrained hinges. Many researchers have examined the aeroelastic stability of this simple blade configuration. For example, Peter[4] and Kaza and Kvaternik[5] investigated the aeroelastic stability of two-degree flap-lag blade in forward flight. An improvement for this type of modelling is to introduce a third degree of motion, i.e., feather rotation. A better representation for a hingeless blade is to treat it as an elastic beam. As an example, Friedmann and Kottapalli[6] have investigated aeroelastic stability of flap bending, lag bending and torsion of an elastic hingeless blade in forward flight. In the present paper, a simple blade representation consisting of three degrees of motion, flap, lag and feather rotations, is used to study the stability phenomena in forward flight.

There are many forms of vehicle trim solutions available in literature. Johnson[7], for example, presented in a summary form many trim options. For free flight conditions, the control settings and the vehicle angles are determined from the satisfaction of three force and three moment equilibrium equations. One of the popular trim procedure is to neglect altogether yawing moment equilibrium equation and thereby neglect the influence of tail rotor on solution. This form of trim solution is used in the present paper. The next simple form of trim procedure[6] is to neglect the lateral force equilibrium equation, and thereby exclude the determination of lateral shaft tilt angle (ϕ_s) from equilibrium equations. Generally, this may cause only slight influence on trim and

stability solutions, because the shaft lateral tilt angle does not introduce any vertical flow component on the blade. Some researchers[4,5,8] have simplified the trim procedure further by assuming that the vehicle center of gravity lies at the rotor hub, and thereby neglect the equilibrium of pitching and rolling moments of the vehicle. This will cause cyclic flap angles β_{1c} and β_{1s} (with respect to hub plane) to be zero. Here, the control settings and shaft angle α_s are calculated from the vertical and longitudinal force equilibrium equations. This may again have a small influence on trim solution for free level flight conditions at low forward speeds. At high forward speeds, the cyclic flap angles are not small and therefore must not be neglected. Another form of trim procedure called moment trim is often used by many researchers[4,9,10], and for this the solution is calculated from the rolling moment and the pitching moment equilibrium equations. The force equilibrium equations are not considered. Here, the rotor cyclic controls (θ_{1c} and θ_{1s}) are calculated for a prescribed shaft angle α_s. Some people refer it as a wind tunnel trim and it can be quite different from propulsive trim[4,6].

The blade time dependent positon is calculated from blade equilibrium equations. These are coupled equations and contain nonlinear geometric terms as well as periodic terms. The objective is to calculate steady periodic response solution. In the present paper, the nonlinear equations are solved in the rotating frame in an iterative procedure based on Floquet theory[11]. A somewhat similar type of quasilinearization procedure was used by Friedmann and Kottapalli[6]. The solution contains all harmonics for flap, lag and torsion response amplitudes. Another popular method, harmonic balancing[12] (Fourier Series) is quite commonly used to calculate the blade steady response where response is assumed periodic and consists of sum of finite harmonics. This procedure gets quite involved for coupled systems with nonlinearities. Quite frequently, researchers[4] have obtained simple response solution using harmonic balance method where the flap response is assumed to undergo a single harmonic motion (β_0, β_{1c} and β_{1s}) and the lag and torsion responses are neglected. In literature[1,2], the importance of accurate determination of blade equilibrium position on blade stability has been pointed out, including nonlinear terms as well as higher blade harmonics.

For stability analysis, the perturbation equations of motion are linear about the blade equilibrium position and these equations contain many periodic terms. These linearized equations are solved using three different approaches in the present paper. The first approach[6] is to analyze the stability of the blade in the rotating reference frame using Floquet transition matrix theory. This approach is applicable if the inflow is assumed to be steady. The second and third approach analyze the stability or rotor perturbation equations in the fixed reference frame. It is assumed that the rotor is tracked and all the blades are identical. The blade equations in the rotating reference frame are transformed to the fixed reference frame as rotor equations using Fourier coordinate transformation[13]. In the present paper, these transformations are performed numerically and thus the working through the laborious algebraic expressions is avoided. In the second approach, the rotor equations in the fixed frame are solved using Floquet transition matrix theory. Through the coordinate transformation, many periodic terms present in the rotating frame get cancelled out in the fixed frame. Therefore, the rotor equations in the fixed frame contain only selected periodic terms, for example, third harmonic for three-bladed rotor and second and fourth harmonic for four-bladed rotor. In the third approach[14], a constant coefficient approximation is made by averaging out periodic terms and solving the resulting equations.

In all these three approaches an eigenanalysis is made and the nature of eigenvalues explains the stability of the blade. Another commonly used method[15] is numerical integration of complete equations. This approach is though simple in implementation, but is quite heavy from computation point of view.

For trim and response solutions, the quasi-steady approximation is used for the determination of aerodynamic loads. For the perturbation solution, the unsteady aerodynamics effects can be important and these are introduced in an approximate manner, through a dynamic inflow modelling. The effect of dynamic inflow on coupled flap-lag two degrees of motion in forward flight has been investigated earlier[9-10] and has been shown to be quite important for blade stability. In the present paper, the influence of inflow dynamics has been investigated for a coupled flap-lag-torsion motion with improved trim and response solutions. The dynamic inflow modelling is based on the actuator disk theory. This necessitates the transformation of blade aerodynamic forces to the fixed reference frame and therefore only second and third approach can be conveniently used to analyze blade stability.

In the paper, the effects of several parameters on blade stability is examined, including, structural coupling, pitch-flap coupling, pitch-lag coupling, lag stiffness, torsion stiffness, steady inflow distribution, dynamic inflow, blade response and constant coefficient approximation.

EQUATIONS OF MOTION

The blade is assumed to undergo three degrees of motion: rigid body flap, lag and feather rotations about hinges at the blade root, with hinge springs to obtain arbitrary natural frequencies. The hinge sequence is flap inboard, lag, and then feather outboard. The flap angle β is positive up the lag angle ζ is positive aft (opposite to rotation) and the feather angle θ is positive nose up. The equations of motion are derived for this configuration, and in general, terms up to second order are retained in the flap and lag equations and terms up to third order are retained in the feather equation. The equations are

Flap Equation:

$$\ddot{\beta} + \nu_\beta^2\beta + 2\omega_\beta\zeta_\beta\dot{\beta} - 2\beta\dot{\zeta} - \frac{3}{2}\frac{X_I}{R}(\ddot{\theta} + \theta)$$

$$+ I_f^*(\zeta\ddot{\theta} + \zeta\theta) + \frac{R_S}{\Delta}(\omega_\zeta^2 - \omega_\beta^2)\sin\theta\cos\theta$$

$$\zeta = \frac{M_\beta}{I_b\Omega^2} + \omega_\beta^2\beta_p \qquad (1)$$

Lag Equation:

$$\ddot{\zeta} + \nu_\zeta^2\zeta + 2\omega_\zeta\zeta_L\dot{\zeta} + 2\beta\dot{\beta} - \frac{3}{2}\frac{X_I}{R}(\theta\ddot{\theta} + 2\beta\dot{\theta})$$

$$+ I_f^*\beta\theta + \frac{R_S}{\Delta}(\omega_\zeta^2 - \omega_\beta^2)\sin\theta\cos\theta\cdot\beta = M\zeta/I_b\Omega^2$$

Feather Equation:

$$I_f^*(\ddot{\theta} + \nu_\theta^2\theta + 2\omega_\theta\zeta_\theta\dot{\theta} + \zeta\ddot{\beta} + \beta\zeta)$$

$$+ \frac{3}{2}\frac{X_I}{R}(-\theta\ddot{\zeta} + 2\frac{X_I}{R}\ddot{\theta} - \ddot{\ } + 2\beta\dot{\zeta} - \beta) = \frac{M_\theta}{I_b\Omega^2}$$

$$+ I_f^*\omega_\theta^2\theta\ \text{con}$$

where I_f^* is the ratio of the feathering inertia to flapping inertia; X_I is the chordwise offset of the center of gravity from the pitch axis (positive aft), the ζ_β ζ_L and ζ_θ are the viscous damping coefficients; the ω_β, ω_ζ and ω_θ are the nonrotating natural frequencies of the blade (divided by rotational speed Ω) and β_p is the precone angle. The M_β, M_ζ, M_θ are the aerodynamic flap, lag and feather moments respectively. For a uniform blade the nondimensional rotating frequencies are given as

$$\nu_\beta^2 = 1 + \frac{3}{2}\frac{e}{1-e} + \frac{R_S}{\Delta}(\omega_\beta^2 + R_S(\omega_\zeta^2 - \omega_\beta^2)\sin^2\theta)$$

$$\nu_\zeta^2 = \frac{3}{2}\frac{e}{1-e} + \frac{R_S}{\Delta}(\omega_\zeta^2 - R_S(\omega_\zeta^2 - \omega_\beta^2)\sin^2\theta)$$

$$\nu_\theta^2 = 1 + \omega_\theta^2$$

$$\Delta = 1 + R_S(1-R_S)\frac{\omega_\beta^2 - \omega_\zeta^2}{\omega_\beta^2\,\omega_\zeta^2}\sin^2\theta$$

The e is the hinge offset (divided by radius of the blade) and R_S is the structural coupling parameter. A simple means of representing structural coupling effect in the rigid blade representation is illustrated in Fig. 1(a). It is used to characterize the hub to blade stiffness and is defined as

$$R_S = \frac{K_\zeta}{K_{\zeta_B}} = \frac{K_\beta}{K_{\beta_B}} \quad \text{where } K_\beta = \frac{K_{\beta_B}K_{\beta_H}}{K_{\beta_B}+K_{\beta_H}},\ K_\zeta = \frac{K_{\zeta_B}K_{\zeta_H}}{K_{\zeta_B}+K_{\zeta_H}}$$

K_β, K_ζ are the combined hub and blade stiffnesses in flap and lag directions. The R_S=0 represents the configuration with blade part as rigid and all the flexibility concentrated at the hub. The structural fully coupled is represented by R_S=1 and this idealizes flexible blade with rigid hub. The intermediate values of R_S represent the case where both blade as well as hub are flexible.

Quasisteady airfoil characteristics are used to obtain the aerodynamic forces. The perturbation section aerodynamic forces and pitch moment (in the shaft axis) are

$$\delta F_z = \frac{1}{2}\rho c[\delta U_t\{-\frac{U_p}{V}(U_tC_{\ell_\alpha} - U_pC_{d_\alpha}) + \frac{U_t^2}{V}C_\ell + C_\ell V$$

$$- C_d\frac{U_pU_t}{V}\} + \delta U_p\{-\frac{U_t}{V}(U_tC_{\ell_\alpha} - U_pC_{d_\alpha}) + \frac{U_pU_t}{V}C_\ell$$

$$- C_dV - U_p^2/V\,C_d\} + \delta\theta\{V(U_tC_{\ell_\alpha} - U_pC_{d_\alpha})\}]$$

$$\delta F_x = \frac{1}{2}\rho c[\delta U_t\{\frac{U_p}{V}(U_pC_{\ell_\alpha} + U_tC_{d_\alpha}) + \frac{U_pU_t}{V}C_\ell + C_dV$$

$$+ \frac{U_t^2}{V}C_J\} + \delta U_p\{-\frac{U_t}{V}(U_pC_{\ell_\alpha} + U_tC_{d_\alpha}) + \frac{U_p^2}{V}C_\ell$$

$$+ C_\ell V + \frac{U_pU_t}{V}C_d\} + \delta\theta\{V(U_pC_{\ell_\alpha} + U_tC_{d_\alpha})\}]$$

$$\delta M_a = \frac{1}{2}\rho c\,[\delta U_t\{2U_t(C_m - \frac{X_A}{c}C_\ell) + U_pC_{m_\alpha} - \frac{X_A}{c}U_pC_{\ell_\alpha}\}$$

$$+ \delta U_p\{2U_p(C_m - \frac{X_A}{c}C_\ell) - U_tC_{m_\alpha} + \frac{X_A}{c}U_tC_{\ell_\alpha}\}$$

$$+ \delta\theta\{V^2(C_{m_\alpha} - \frac{X_A}{c}C_{\ell_\alpha})\}] \qquad (2)$$

where X_A is the chordwise offset of the aerodynamic center from elastic axis (positive aft), c is the chord, V is the resultant velocity and U_p and U_t are airflow velocity components in tangential and normal directions (Fig. 1(b)). The steady and perturbation flow components for forward flight are

Steady:

$$U_t = \{x(1-e) - x(1-e)\dot{\zeta} + \mu\sin\psi - \zeta\mu\cos\psi\}$$

$$U_p = \{\lambda - x(1-e)\beta\zeta + x(1-e)\dot{\beta} + \mu\beta\cos\psi\}$$

Perturbation: (3)

$$\delta U_t = \{\delta\zeta\mu\cos\psi - x(1-e)\delta\dot{\zeta}\}$$

$$\delta U_p = \{-x(1-e)\beta\delta\zeta - x(1-e)\zeta\delta\beta + x(1-e)\delta\dot{\beta} +$$

$$\mu\delta\beta\cos\psi - \frac{c}{R}(\frac{1}{2} + \frac{X_A}{c})\dot{\delta\theta}\}$$

The perturbation aerodynamic moments required for the stability analysis are written as

$$\delta M_\beta = \int_e^B x \cdot \delta F_z \cdot dx$$

$$\delta M_\zeta = \int_e^B x \cdot \delta F_x \, dx \qquad (4)$$

$$\delta M_\theta = \int_e^B \delta M_a \, dx + \int_e^B M_{NC} \, dx$$

where M_{NC} is the noncirculatory aerodynamic pitch moment and is expressed as

$$M_{nc} = \frac{1}{4}\pi\rho\Omega^2 c^3 R \left[\ddot{\beta}\left(\frac{1}{4} + \frac{X_A}{c}\right) - \frac{1}{4}\frac{c}{R}\left(\frac{2X_A}{c} + \frac{3}{8}\right)\right.$$
$$+ \dot{\beta}\left\{\mu\cos\psi\left(\frac{1}{4} + \frac{X_A}{c}\right) - \frac{1}{4}\frac{c}{R}\left(\frac{2X_A}{c} + \frac{3}{8}\right)\right\}$$
$$- \dot{\theta}\left\{(x+\mu\sin\psi)\left(\frac{1}{2} + \frac{X_A}{c}\right)\right\} \qquad (5)$$
$$\left. - \theta\left\{\frac{x}{4} + \left(\frac{1}{2} + \frac{X_A}{c}\right)\mu\sin\psi\right\}\right]$$

where x is the nondimensional distance from the hub and μ is the advance ratio ($\bar{V}\cos\alpha_s/\Omega R$).

The final blade equations of motion in forward flight can be written as

$$\underset{\sim}{M}_r(\psi)\ddot{\underset{\sim}{X}}_r + \underset{\sim}{C}_r(\psi)\dot{\underset{\sim}{X}}_r + \underset{\sim}{K}_r(\psi)\underset{\sim}{X}_r = \underset{\sim}{F}_{NL}(\psi, \underset{\sim}{X}_r, \dot{\underset{\sim}{X}}_r) \qquad (6)$$

where the inertia matrix $\underset{\sim}{M}_r$, the damping matrix $\underset{\sim}{C}_r$ and stiffness matrix $\underset{\sim}{K}_r$ contain periodic terms. The vector $\underset{\sim}{X}_r$ consists of three states; flap, lag and torsion deflections in the rotating system. The (*) shown in the equations refers differentiations with respect to ψ and ψ is the azimuth angle (nondimensional time, Ωt). All the geometric nonlinearities are put into the force vector $\underset{\sim}{F}_{NL}$. The blade response is calculated from the solution of above equations.

For the stability solution, the flutter motion is assumed to be a small perturbation about the blade equilibrium position.

$$\underset{\sim}{X}_r = \underset{\sim}{X}_r + \delta\underset{\sim}{X}_r \qquad (7)$$

The final linearized perturbed equations are obtained as

$$\underset{\sim}{M}_r^p(\psi)\delta\ddot{\underset{\sim}{X}}_r + \underset{\sim}{C}_r^p(\psi, \underset{\sim}{X}_r, \dot{\underset{\sim}{X}}_r)\delta\dot{\underset{\sim}{X}}_r + \underset{\sim}{K}_r^p(\psi, \underset{\sim}{X}_r, \dot{\underset{\sim}{X}}_r)\delta\underset{\sim}{X}_r = 0 \qquad (8)$$

The perturbation inertia matrix $\underset{\sim}{M}_r^p$, damping matrix $\underset{\sim}{C}_r^p$, stiffness matrix $\underset{\sim}{K}_r^p$ also contain periodic terms. To determine blade stability one needs blade response solution. To calculate this blade response solution one needs the vehicle trim solution.

VEHICLE TRIM SOLUTION

The propulsion trim which is described here simulates the free flight condition. The trim solution in forward flight involves the calculations of pilot-control setting as well as the vehicle orientation for a prescribed flight conditions. For a specified weight coefficient C_w and a fixed forward speed (μ) the trim solution evaluates β_0, β_{1C}, β_{1s}, θ_0, θ_{1C}, θ_{1s}, α_{HP}, ϕ_s and λ. The trim solution is calculated from the vehicle equilibrium equations. Fig. 1(c) shows the forces and moments acting on the vehicle.

Vertical force equilibrium:

$$W - T\cos(\alpha - \theta_{FP})\cos\phi_s + D\sin\theta_{FP} - H\sin(\alpha - \theta_{FP}) + Y\sin\phi_s = 0 \qquad (9)$$

Longitudinal force equilibrium:

$$D\cos\theta_{FP} + H\cos(\alpha - \theta_{FP}) - T\sin(\alpha - \theta_{FP}) = 0 \qquad (10)$$

Lateral force equilibrium:

$$Y_f + Y\cos\phi_s + T\sin\phi_s = 0 \qquad (11)$$

Pitching moment:

$$M_y + M_{yf} - W(X_{cg} - h\sin\alpha) - D\cos(\alpha + \theta_{FP})h - D\sin(\alpha + \theta_{FP})\cdot X_{cg} = 0 \qquad (12)$$

Rolling moment:

$$M_x + M_{xf} + Y_f \cdot h\cos\phi_s + Y_f Y_{cg}\sin\phi_s + Wh\sin\phi_s - W Y_{cg}\cos\phi_s = 0 \qquad (13)$$

Where T is the rotor thrust and Y and H are the side and drag forces. These are five vehicle equilibrium equations. For trim solution one also needs rotor equilibrium equations in simplified form. These are

$$\frac{1}{2\pi}\int_0^{2\pi} (\text{Flapping equation})\, d\psi = 0 \qquad (14)$$

$$\frac{1}{2\pi}\int_0^{2\pi} (\text{Flapping equations})\cos\psi\, d\psi = 0 \qquad (15)$$

$$\frac{1}{2\pi}\int_0^{2\pi} (\text{Flapping equations})\sin\psi\, d\psi = 0 \qquad (16)$$

The induced inflow is related to the rotor thrust as

$$\lambda = \mu \tan \alpha + \frac{C_T}{2\sqrt{\mu^2+\lambda^2}} (1+k_x \cdot x \cos \psi + K_y \cdot x \sin \psi) \quad (17)$$

where K_x and K_y are obtained from Drees model[13] and is expressed as

$$K_x = 4/3[(1-1.8\mu^2)\sqrt{1 - (\lambda/\mu)^2} - \lambda/\mu]$$

$$K_y = -2\mu$$

For hover $K_x = K_y = 0$

These are nine equations with nine unknowns (β_0, β_{1c}, β_{1s}, θ_0, θ_{1c}, θ_{1s}, λ, α, ϕ_s) and these are solved numerically by iterative method.

BLADE RESPONSE SOLUTION

The blade response solution involves the determination of time dependent blade position and is calculated from the blade equations (6). For the calculation of response solution one needs vehicle trim solution. The nonlinear response solution is obtained from nonlinear periodic equations (6) using Floquet theory[11]. These equations are expressed in the state vector form

$$\dot{\underset{\sim}{Y}}_r - \underset{\sim}{A}(\psi)\underset{\sim}{Y}_r = \underset{\sim}{G}_r(\psi, \underset{\sim}{Y}_r, \dot{\underset{\sim}{Y}}_r) \quad (18)$$

where $\underset{\sim}{Y}_r$ is the state variable vector involving six states.

First a linear solution is calculated after dropping all nonlinear terms. For this the initial conditions are calculated from Floquet theory as

$$\underset{\sim}{Y}(0) = (\underset{\sim}{I} - \underset{\sim}{Q}(2\pi))^{-1} \underset{\sim}{Y}_e(2\pi) \quad (19)$$

where $\underset{\sim}{Y}_e(2\pi)$ is the complete solution after one revolution with rest initial conditions and $\underset{\sim}{Q}(2\pi)$ is the Floquet transition matrix. For numerical integration of the equations, a fourth order Runge-Kutta algorithm is used. The next step is to obtain the initial conditions for the complete nonlinear problem. This is done in an iterative manner. As a first guess, the above linear solution is used as an initial vector $\underset{\sim}{Y}_e(0)$ for the nonlinear solution and the complete response $\underset{\sim}{Y}_e(2\pi)$ after one revolution is calculated. The updated Floquet transition matrix $\underset{\sim}{Q}$ is function of response amplitude and is calculated by perturbing the estimated initial conditions $\underset{\sim}{Y}_e(0)$ by a small perturbation vector $\underset{\sim}{\varepsilon}$.

$$\underset{\sim}{Q}(2\pi) = [\frac{1}{\varepsilon_1}(\underset{\sim}{Y}^{(1)}(2\pi) - \underset{\sim}{Y}_e(2\pi)), \frac{1}{\varepsilon_2}(\underset{\sim}{Y}^{(2)}(2\pi) - \underset{\sim}{Y}_e(2\pi)), \ldots, \frac{1}{\varepsilon_6}(\underset{\sim}{Y}^{(6)}(2\pi) - \underset{\sim}{Y}_e(2\pi))] \quad (20)$$

Where $\underset{\sim}{Y}^{(i)}(2\pi)$ is the response with initial conditions of

$$\underset{\sim}{Y}_e(0) = \begin{Bmatrix} 0 \\ 0 \\ \varepsilon_i \\ 0 \end{Bmatrix} + \underset{\sim}{Y}_e(0)$$

So a new set of initial conditions for the nonlinear analysis are obtained

$$\underset{\sim}{Y}(0) = \underset{\sim}{Y}_e(0) + [\underset{\sim}{I} - \underset{\sim}{Q}]^{-1} (\underset{\sim}{Y}_e(2\pi) - \underset{\sim}{Y}_e(0)) \quad (21)$$

This procedure is repeated till a converged set of initial conditions is obtained. Typically it takes about 2 to 3 iterations to obtain converged solution. Once the initial conditions $\underset{\sim}{Y}(0)$ are obtained, then the total response $\underset{\sim}{Y}(\psi)$ for any time in a revolution is calculated numerically using time integration (Runge Kutta). This gives us the nonlinear equilibrium deflection of the blade along the azimuth.

FLUTTER SOLUTION

The linearized perturbed equations of motion (8) is written in the state vector form as

$$\dot{\delta\underset{\sim}{Y}}_r = A(\underset{\sim}{Y}_r, \dot{\underset{\sim}{Y}}_r, \psi)\delta\underset{\sim}{Y}_r \quad (22)$$

where $\underset{\sim}{Y}_r$, $\dot{\underset{\sim}{Y}}_r$ are the blade equillibrium position in the rotating reference frame and $\delta\underset{\sim}{Y}_r$ and $\dot{\delta\underset{\sim}{Y}}_r$ are perturbation states. These linearized equations are solved for stability using Floquet transition matrix theory[13]. Here the eigenvalues of transition matrix of A can be written in characteristic exponents form

$$\lambda_k = \alpha_k + i\omega_k \quad (23)$$

and the mode in stable when $\alpha_k < 0$.

For the perturbation solution the unsteady aerodynamics effect can be important and these are introduced in an approximate manner, through a dynamic inflow modelling. The wake inflow is perturbed about the steady inflow λ

$$\lambda = \lambda + \delta\lambda \quad (24)$$

where $\delta\lambda$ is the perturbed inflow component.

A linear variation of perturbed inflow is used

$$\delta\lambda = \delta\lambda_0 + \delta\lambda_{1C} \times \cos \psi + \delta\lambda_{1s} \times \sin \psi \quad (25)$$

The dynamic inflow components $\delta\lambda_0$, $\delta\lambda_{1C}$, $\delta\lambda_{1s}$ are related to rotor unsteady aerodynamic forces and moments

$$m\dot{\delta\lambda}^{*} + \ell^{-1}\,\delta\lambda = \delta F \qquad (26)$$

where $\delta F = \sum_{i=1}^{N_b} \begin{Bmatrix} \delta C_T \\ \delta C_{m_x} \\ \delta C_{m_y} \end{Bmatrix}_i \qquad \delta\lambda = \begin{Bmatrix} \delta\lambda_0 \\ \delta\lambda_{1s} \\ \delta\lambda_{1c} \end{Bmatrix}$

The δC_T, δC_{m_x}, δC_{m_y} are the perturbed thrust, roll moment and pitch moment and these are obtained for the ith blade. The $\underset{\sim}{m}$ and $\underset{\sim}{\ell}^{-1}$ matrices used here are evaluated analytically based on the actuator disk theory in Ref. 16. The nonzero elements of $\underset{\sim}{m}$ and $\underset{\sim}{\ell}$ are

$$m_{11} = \frac{128}{75\pi} \qquad m_{22} = m_{33} = -\frac{16}{45\pi}$$

$$\ell_{11} = \frac{1}{2v} \qquad \ell_{22} = \frac{\ell_{33}}{\sin\alpha} = -\frac{4}{1+\sin\alpha}\cdot\frac{1}{v}$$

$$\ell_{13} = \ell_{31} = \frac{15\pi}{64}\quad\frac{1-\sin\alpha}{1+\sin\alpha}\cdot\frac{1}{v}$$

where $v = \dfrac{\mu^2+\lambda(\lambda+\lambda_i)}{\sqrt{\mu^2+\lambda^2}}$ and $\alpha = \tan^{-1}\left(\dfrac{\lambda}{\mu}\right)$

λ_i is the induced inflow due to steady rotor thrust. This model gives a quite accurate description of dynamic inflow as concluded in reference 9.

The disk loading is approximated in terms of the blade loading, δF_z as

$$\delta C_T = \frac{\sigma a}{\gamma N_b} \sum_{k=1}^{N_b} \int_e^1 (\delta\bar{F}_z)_k \, dx$$

$$\delta C_{M_x} = -\frac{\sigma a}{\gamma N_b} \sum_{k=1}^{N_b} \int_e^1 (\delta\bar{F}_z)_k \, x\,dx \sin\psi_k \qquad (27)$$

$$\delta C_{M_y} = -\frac{\sigma a}{\gamma N_b} \sum_{k=1}^{N_b} \int_e^1 (\delta\bar{F}_z)_k \, x\,dx \cos\psi_k$$

With the inclusion of dynamic inflow, it is convenient to analyze blade stability in the fixed reference frame. The coupled blade equations are transformed to the fixed reference frame from rotating frame using Fourier co-ordinate transformation[13]. For four bladed rotor (N_b=4)

$$\frac{1}{N_b}\sum_{m=1}^{N_b} (\text{Differential equation}) \begin{Bmatrix} 1 \\ 2\cos\psi_m \\ 2\sin\psi_m \\ (-1)^m \end{Bmatrix} = 0 \qquad (28)$$

These transformations are carried out numerically. The final equations of motion in fixed co-ordinate frame can be written as

$$\dot{\delta Y}_F^{*} = \underset{\sim}{A}_f(\psi)\;\delta Y_F + \underset{\sim}{N}_f(\psi)\,\delta\lambda \qquad (29)$$

The unsteady force δF in dynamic inflow equations is given as

$$\delta\bar{F} = \underset{\sim}{B}_1(\psi)\,\delta Y_F + \underset{\sim}{B}_2(\psi)\,\delta\lambda \qquad (30)$$

Putting together the rotor equations with the inflow equation, one gets

$$\begin{Bmatrix} \dot{\delta Y}_f^{*} \\ \dot{\delta\lambda}^{*} \end{Bmatrix} = \begin{bmatrix} \underset{\sim}{A}_f(\psi) & \underset{\sim}{N}_f(\psi) \\ \underset{\sim}{M}^{-1}\underset{\sim}{B}_1 & \underset{\sim}{M}^{-1}\underset{\sim}{B}_2 - \underset{\sim}{M}^{-1}\underset{\sim}{\ell}^{-1} \end{bmatrix} \begin{Bmatrix} \delta Y \\ \delta\lambda \end{Bmatrix} \qquad (31)$$

The above equations in the fixed frame contain only selected harmonics, for example third harmonic for 3 bladed rotor, second and fourth for 4 bladed rotor. These linearized periodic equations are solved using Floquet transition matrix theory and constant coefficient approximation approach. In the constant coefficient approximation approach the periodic terms are averaged out by applying the operator

$$\frac{1}{2\pi}\int_0^{2\pi} (\text{------})\, d\psi \qquad (32)$$

and then solved as an eigenvalue problem.

RESULTS AND DISCUSSION

The aeroelastic stability is examined for a four-bladed rotor with Lock number γ = 5.0, solidity ratio σ = 0.05, feather inertia to flap ratio I_f^{*}=0.0003 and with zero precone. The blade offsets such as the X_I, the chordwise center of gravity offset from pitch axis in terms of radius and X_A aerodynamic centre offset from elastic axis are set to zero. The

fuselage centre of gravity lies on the shaft axis and is assumed to be at a distance 0.2R below the rotor center. The aerofoil characteristics used are

$$C_\ell = 5.7\alpha$$

$$C_d = 0.01$$

$$C_m = -0.02$$

The helicopter drag coefficient in terms of flat plate area ratio ($f/\pi R^2$) of .01 is used. The blade flap and torsion frequencies (rotating) are 1.15/rev and 5.0/rev respectively. Two different lag frequencies are used; 0.57/rev for soft inplane rotor and 1.4/rev for stiff inplane rotor. The soft inplane rotor configuration was taken as a matched stiffness case ($\omega_\beta = \omega_\zeta$).

First, results were calculated for some selected cases to make comparison with those of other authors for identical conditions. The vehicle trim was calculated for uniform inflow conditon with the center of gravity lying at the rotor hub (h=0) and the results obtained were identical to those of Ref. 18. The blade stability of two-degree flap-lag blade was calculated using simple response solution (single flap harmonic) and for uniform steady inflow condition. The lag damping values calculated for various flight conditions were quite identical to those of Ref. 4. The inclusion of dynamic inflow on the stability of this two-degree motion blade was checked with the results of Ref. 9, and again, the comparison was quite satisfactory. Then, the flap-lag-torsion stability results were calculated for soft and stiff inplane configurations for steady inflow conditions. For perturbation solution, a nonlinear equilibrium position was used. The stability results showed some comparable trends with those of Ref. 6, in which results are obtained with improved structural modelling for the blade (elastic beam).

Figs. 2(a) and 2(b) show the vehicle trim solutions for $\frac{C_W}{\sigma}$ of .2 and .1 respectively. The propulsive trim parameters θ_0, θ_{1C}, θ_{1S}, α_{HP}, ϕ_S, λ, β_0, β_{1C}, β_{1S} are plotted for different forward speeds (in terms of advance ratio $\mu = \bar{V}/\Omega R$). The solution is calculated iteratively from nonlinear equilibrium equations (large angles). The flight path angle θ_{FP} is assumed to be zero. For steady inflow, a linear distribution model (Drees) is used. These trim parameters are defined in the hub plane axes system and so the cyclic flap angle β_{1C} is small for even large μ. For larger μ, the shaft has to tilt more to compensate the increase in parasite drag and hence α_{HP} increases with μ and thereby cause inflow λ to increase. For large thrust levels C_W/σ, control requirements are large but the angle α_{HP} is small. The reason for lower shaft angle at high C_W/σ is due to the fact that, for same parasite drag (for a given forward speed) the shaft has to tilt less to balance the parasite drag as the thrust magnitude is more. It is also observed that trim calculated from linearized equilibrium equations (small angles assumption) is quite close to the above nonlinear solution except for large advance ratios. The influence of inflow distribution is primarily on longitudinal and lateral cyclic pitch θ_{1S}, θ_{1C}. The effect of uniform inflow for $\frac{C_W}{\sigma} = 0.1$ is shown by dotted line in Fig. 2(b). The effect of inflow distribution on other trim parameters is quite small.

Figs. 3(a)-(c) present time dependent equilibrium position of blade for one complete revolution. The response solution in terms of flap, lag and torsion deflections (angles) is calculated iteratively from nonlinear blade equations (rotating frame) using the floquet theory described earlier. These results correspond to a $\frac{C_W}{\sigma} = 0.1$ and advance ratio $\mu = 0.2$. For comparison, the linear response solution (dotted) is also presented. The geometric nonlinearities are important for lag response and play less important role in flap and torsion response calculations.

For numerical results, a convergence study was conducted to determine time steps needed in one revolution for time integration (Runge-Kutta) for both response as well as stability calculations using Floquet Theory. It was concluded that 120 time steps are quite adequate for well converged (four significant-digit) response and stability solutions. For stability results, only the lowest damped lag mode is presented. The flap and torsion modes are comparitively high damped modes and are not presented here. The damping in terms of real part of complex eigenvalue, α_ζ is shown. Note $\alpha_\zeta = \zeta_L \omega_\zeta$, where ζ_L damping ratio of lag mode and ω_ζ/Ω is frequency of lag mode nondimensionalized with respect to rotational speed.

In Fig. 4, the effect of torsion flexibility on the blade stability is shown. For these solutions, the simple blade response is used and the stability roots are obtained in the rotating frame with steady uniform inflow conditions. There is a disparity between two results, clearly showing the importance of inclusion of torsion flexibility for blade stability analysis. This has been pointed out by other authors[6].

Fig. 5 shows the effect of blade response solutions on stability. The lag mode damping is calculated using three types of blade equilibrium solutions; these are complete nonlinear solution, linear solution and simple solution. The linear

and nonlinear solutions contain all harmonics for flap, lag and torsion modes whereas the simple solution consists of single flap harmonic only. These solutions are obtained in the rotating frame with steady uniform inflow conditions. Though it is computationally less involved to use simple response solution, the results are poor in accuracy. For accurate results it is needed to use a complete nonlinear blade response solution.

Fig. 6 presents the influence of steady inflow distribution on the blade stability. These solutions are obtained in the fixed frame with dynamic inflow included. In the figure the damping of the lowest damped, low frequency cyclic lag mode (regressive mode) is presented. Two types of steady inflow model are used; uniform distribution and linear distribution (Drees). The uniform distribution underpredicts lag damping. For subsequent results, the linear inflow model (Drees) is used.

Figs. 7 and 8 present the damping of low frequency cyclic lag mode for different advance ratio μ. Three sets of results are shown and these respectively represent dynamic inflow Floquet results (full line), dynamic inflow constant coefficient approximation results (big dots) and steady inflow results (small dots). In Figures 7(a) and 7(b), the stability results are shown for stiff inplane rotor for $C_W/\sigma = .1$ and .2 respectively. For this case the low frequency mode is a regressive mode. The constant coefficient approximation is quite satisfactory for small advance ratios μ. The inclusion of dynamic inflow is important for low forward speeds. This shows that for large forward speeds unsteady aerodynamic effects are not important and quasisteady approximation is quite adequate for blade stability analysis. At large thrust levels the influence of dynamic inflow and constant coefficient approximation is large because of larger aerodynamic forces involved. Figs. 8(a) and 8(b) show the blade stability results for soft inplane rotor for C_W/σ of .1 and .2 respectively. For this case the low frequency mode is a progressive mode. Again for the matched stiffness configuration, the results are quite identical to the stiff configuration. Constant coefficient approximation less satisfactory for high advance ratios, the dynamic inflow inclusion is more important for low advance ratios.

In Figs. 9 and 10 the effect of structural coupling on lag mode stability is presented for stiff inplane and soft inplane rotors respectively for C_W/σ of 0.1. The earlier results were calculated for blades with no structural coupling (R_S=0). This idealizes the configurations with blade part as rigid and all the flexibility concentrated at the hub. The structurally fully coupled is represented by R_S=1 and this idealizes flexible blade with rigid hub. The value of R_S less than 1 represents intermediate cases where both blade as well as hub are flexible. The stability results are obtained using Floquet theory with dynamic inflow effects included. The structural coupling has an important effect on blade stability for stiff inplane rotor. In fact with large structural coupling the blade becomes more stable. This is because with a large structural coupling R_S, the weakly damped lag mode gets coupled with well damped flap mode and thereby stabilizes the lag mode. The effect of structural coupling is negligible on the soft lag configuration and this is because the configuration considered is matched stiffness case. On these figures the results are also plotted with steady linear inflow aerodynamics. For stiff lag rotors, the effect of inclusion of dynamic inflow is large for configurations with zero structural coupling, and the influence is quite stabilizing. With large structural coupling R_S, the effect of dynamic inflow is less and it is destabilizing.

Figs. 11 and 12 show the effect of torsional stiffness on lag mode stability for stiff inplane and soft inplane rotors for C_W/σ of .1. Results are obtained for three different torsional frequencies and these are 2.5, 5 and 10 per revolution. For both soft inplane and stiff inplane rotors, increasing torional stiffness increases lag damping (more stable) for lower forward speeds (low μ) and decrease lag damping (less stable) at higher forward speeds.

The effect of pitch-flap and pitch-lag coupling terms on blade stability is studied by modifying the feather angle in the flap-lag equations (two-degree-of-freedom)

$$\theta_{eff} = \theta - K_{p_\beta}\,\beta - K_{p_\zeta}\,\zeta$$

The pitch-flap coupling K_{p_β} is positive flap up/pitch down, and the pitch-lag coupling is positive lag back/pitch down. These couplings are caused due to torsion dynamics or kinematic couplings. Figs. 13(a) and 13(b) show the influence of pitch-lag coupling on lag mode stability for stiff inplane and soft inplane rotors respectively for C_W/σ of 0.1. The positive pitch-lag coupling stabilizes the low freguency cyclic lag mode for stiff inplane rotors, and destablizes this lag mode for soft inplane rotors. The opposite effect is seen with the negative pitch-lag coupling. A similar type of observation is made for hovering blade stability in Ref. 17. Figs. 14(a) and 14(b) show the effect of pitch-flap coupling on lag mode stability for stiff inplane and soft inplane rotors respectively for C_W/σ of 0.1. A negative pitch-flap coupling reduces the flap frequency, and it produces a

stabilizing effect on lag mode for low forward speeds and a destabilizing effect at higher forward speeds. A positive pitch-flap coupling raises the flap frequency, and it has a comparatively small effect on lag mode stability. Also, it can be seen the effect of pitch-flap coupling on blade stability is much smaller as compared to that of pitch-lag coupling.

CONCLUSIONS

An aeroelastic stability of a simple three-degree-of-freedom blade model in forward flight is examined. The nonlinear time dependent blade equilibrium position is calculated using a quasilinearization procedure based on Floquet theory. The perturbation solution is obtained using Floquet transition matrix theory as well as constant coefficient approximation in the fixed reference frame. The stability results are calculated for both stiff-inplane and soft-inplane blade configurations. The inclusion of torsion degree of motion is important for blade stability. The nonlinear time dependent periodic blade response has a significant influence on blade stability. For steady inflow distribution, the linear variation (Drees) is somewhat stabilizing for lag mode damping as compared to uniform distribution. The effect of dynamic inflow on lag mode stability is small at high forward speeds ($\mu > .3$). The constant coefficient approximation appears satisfactory for low forward speeds ($\mu < .2$). The structural coupling produces stabilizing effect on blade stability for stiff lag rotors. For matched-stiffness configurations, there is no effect of structural coupling on blade stability. Raising of torsional stiffness increases lag mode damping (more stable) at lower forward speeds ($\mu < .15$) and decreases lag damping (less stable) at higher forward speeds ($\mu > .15$). A positive pitch-lag coupling stabilizes the low frequency cyclic lag mode for stiff lag rotors and destabilizes this mode for soft-lag rotors. An opposite effect is seen with negative pitch-lag coupling. The effect of pitch-flap coupling on lag mode damping is small as compared to pitch-lag coupling effect. The negative pitch-flap coupling stabilizes lag mode at low forward speeds and destabilizes it at higher forward speeds. The positive pitch-flap coupling has a little influence on lag mode stability.

REFERENCES

1. Ormiston, R.A., "Investigation of Hingeless Rotor Stability," Vertica, Vol. 7, No. 2, 1983, pp. 143-181.

2. Friedmann, P.P., "Recent Development in Rotoray-Wing Aeroelasticity," Journal of Aircraft, Vol. 14, No. 11, Nov. 1977, pp. 1027-1041.

3. Friedmann, P.P., "Formulation and Solution of Rotary-Wings Aeroelastic Stability and Response Problems," Vertica, Vol. 7, No. 2, 1983, pp. 101-141.

4. Peters, D.A., "Flap-Lag Stability of Helicopter Rotor Blades in Forward Flight," Journal of the American Helicopter Society, Vol. 20, No. 4, Oct. 1975, pp. 2-13.

5. Kaza, K.R.V. and Kvaternik, R.G., "Examination of Flap-Lag Stability of Rigid Articulated Rotor Blades," Journal of Aircraft, Vol. 16, No. 12, December 1979, pp. 876-884.

6. Friedmann, P.P. and Kottapalli, S.B.R., "Coupled Flap-Lag-Torsional Dynamics of Hingeless Rotor Blades in Forward Flight," Journal of the American Helicopter Society, Vol. 27, No. 4, Oct. 1982, pp. 28-36.

7. Johnson, W., "A Comprehensive Analytical Model of Rotorcraft Aerodynamics and Dynamics:Part I," NASATM81182, USAAVRADCOM TR80-A-5, June 1980.

8. Friedmann, P.P. and Shamie, J., "Aeroelastic Stability of Trimmed Helicopter Blades in Forward Flight," Vertica, Vol. 1, No. 3, 1977, pp. 189-211.

9. Gaonkar, G.H., Sastry, V.V.S.S., Reddy, T.S.R., Nagabhushanam, J., Peters, D.A., "The Use of Actuator Disc Dynamic Inflow for Helicopter Flap-Lag Stability," Journal of the American Helicopter Society, Vol. 28, No. 3, July 1983, pp. 79-88.

10. Peters, D.A. and Gaonkar, G.H., "Thoretical Flap-Lag Damping with Various Dynamic Inflow Models," Journal of the American Helicopter Society, Vol. 25, No. 3, July 1980, pp. 29-36.

11. Dugundji, J. and Wendell, H., "Some Analysis Methods for Rotating Systems with Periodic Coefficients," AIAA Journal, Vol. 21, No. 6, June 1983, pp. 890-897.

12. Peters, D.A. and Ormiston, R.A., "Flapping Response Characteristics of Hingeless Rotor Blades by a Generalized Harmonic Balance Method," NASA TN D-7856, Feb. 1975.

13. Johnson, W., "Helicopter Theory," Princeton University Press, Princeton, New Jersey, 1980.

14. Biggers, J.C., "Some Approximation to the Flapping Stability of Helicopter Rotors," Journal of the American Helicopter Society, Vol. 9, No. 4, Oct. 1974, pp. 24-33.

15. Chopra, I., "Dynamic Analysis of Constant-Lift and Free-Tip Rotors," Journal of the American Helicopter Society, Vol. 28, No. 1, Jan. 1983, pp. 24-33.

16. Pitt, D.M. and Peters, D.A., "Theoretical Prediction of Dynamic Inflow Derivatives," Vertica, Vol. 5, No. 1, 1981, pp. 21-34.

17. Ormiston, R.A. and Hodges, D.H., "Linear Flap-Lag Dynamics of Hingeless Helicopter Rotor Blades in Hover," Journal of the American Helicopter Society, Vol. 17, No. 2, April 1972, pp. 1-14.

18. Straub, F.K. and Friedmann, P.P., "A Galerkin type Finite Element method for rotary-wing aeroelasticity," Vertica, Vol. 5, No. 1, 1981, pp. 75-98.

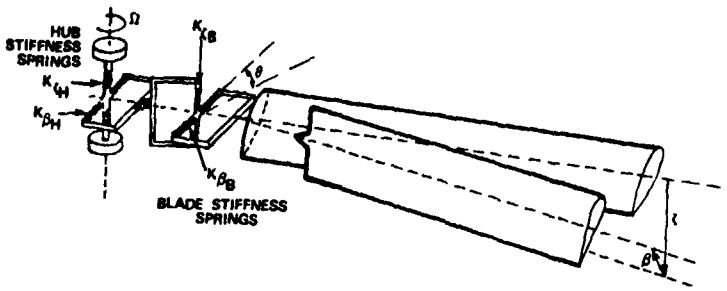

Fig. 1(a) Spring model for elastic blade and hub

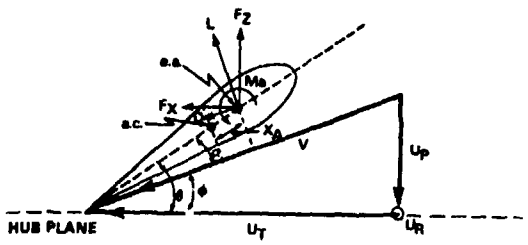

Fig. 1(b) Blade section Aerodynamics

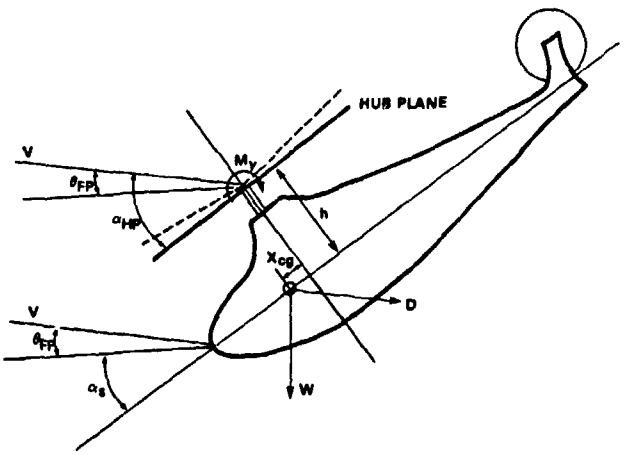

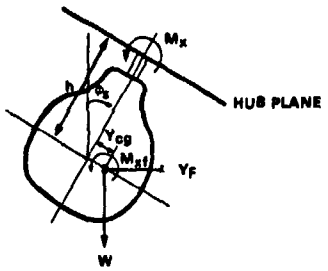

Fig. 1(c) Helicopter in forward flight showing vehicle trim configuration

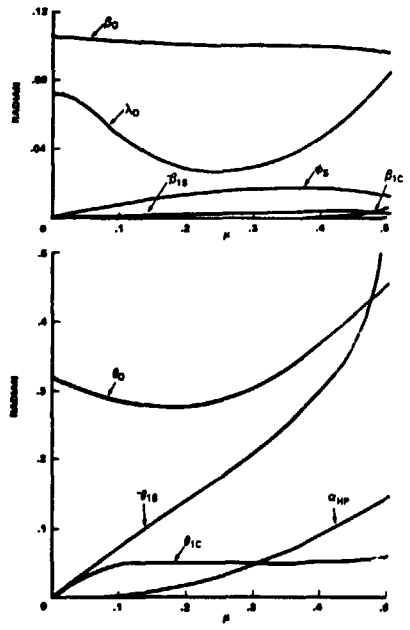

Fig. 2(a) $C_W/\sigma = 0.2$

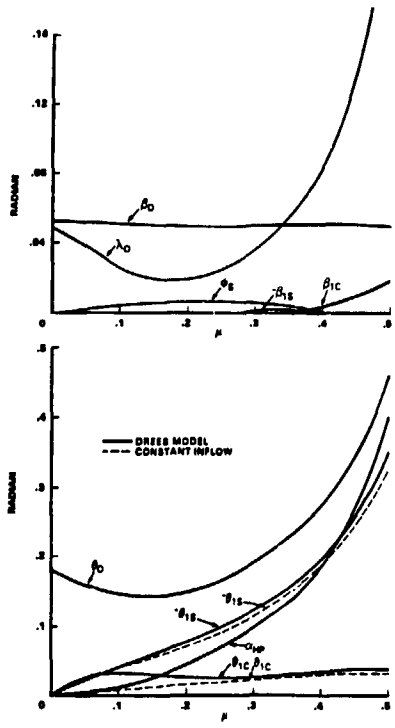

Fig. 2(b) $C_W/\sigma = 0.1$

Fig. 2 Vehicle propulsive trim (γ=5.0, σ=0.05, N_b=4, ν_β=1.15)

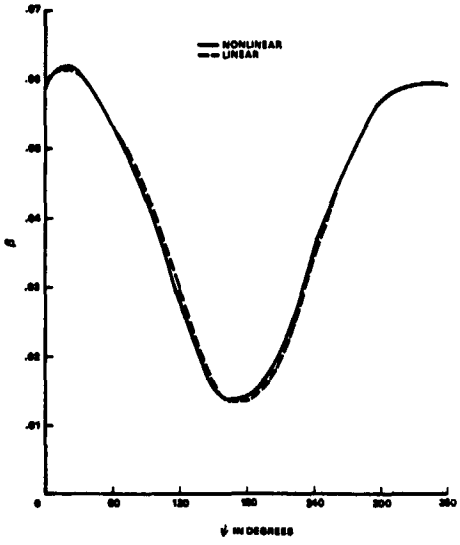

Fig. 3(a) Flap equilibrium angle

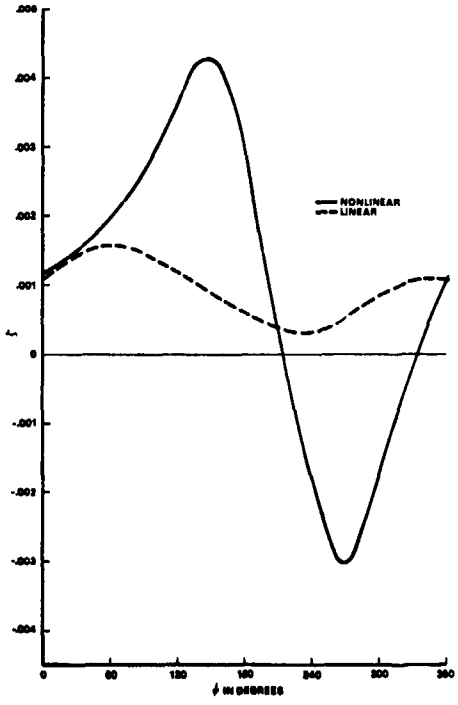

Fig. 3(b) Lag equilibrium angle

Fig. 3 Blade equilibrium position for C_W/σ=0.1 and μ=0.2

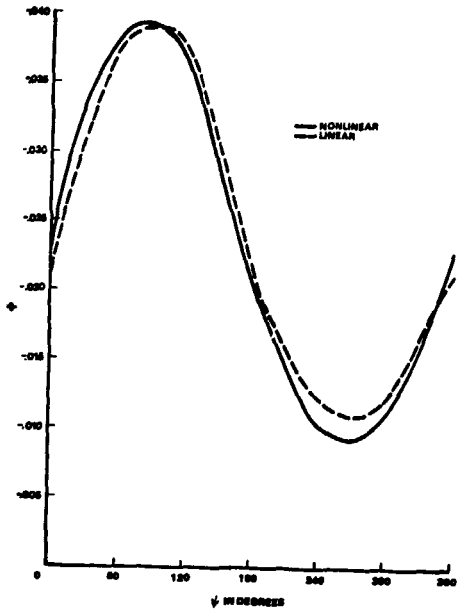

Fig. 3(c) Torsion equilibrium angle

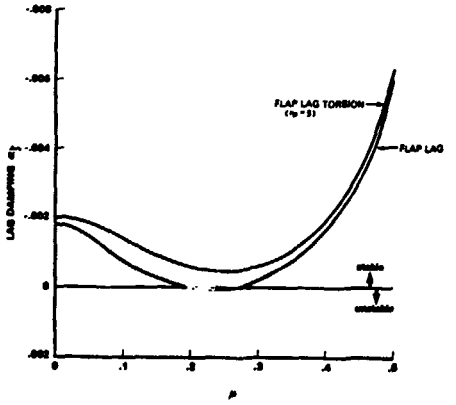

Fig. 4 Effect of torsion degree of freedom on lag mode stability for $C_w/\sigma=0.2$ ($\nu_\beta=1.15$, $\nu_\zeta=1.4$, $R_s=0$, steady uniform inflow)

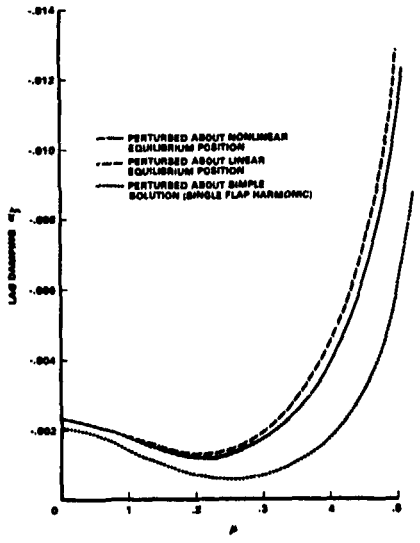

Fig. 5 Effect of blade response solutions on lag mode stability for $C_w/\sigma=0.2$ ($\nu_\beta=1.15$, $\nu_\zeta=1.4$, $\nu_\theta=5$, $R_s=0$, steady uniform inflow)

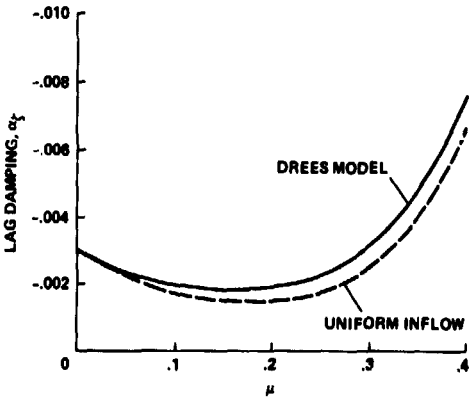

Fig. 6 Effect of steady inflow on low frequency cyclic lag mode (Regressive) stability for $C_w/\sigma=0.1$ ($\nu_\beta=1.15$, $\nu_\zeta=1.4$, $\nu_\theta=5$, $R_s=0$, Dynamic Inflow)

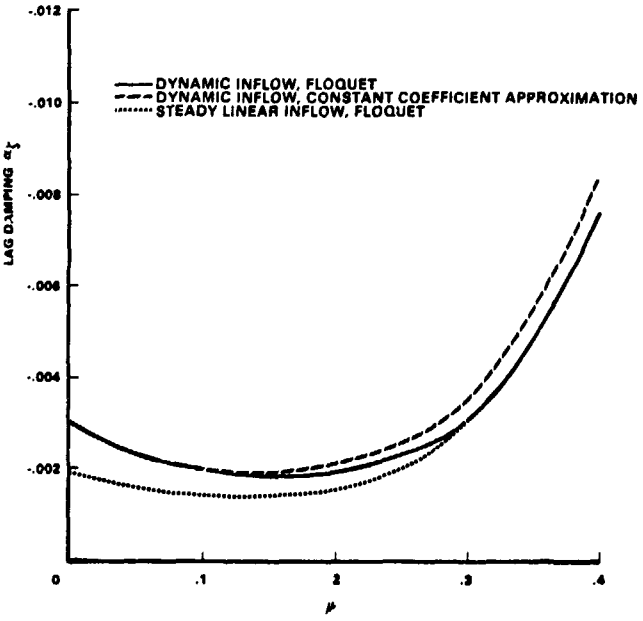

Fig. 7(a) Stiff-lag rotor, $C_w/\sigma=0.1$

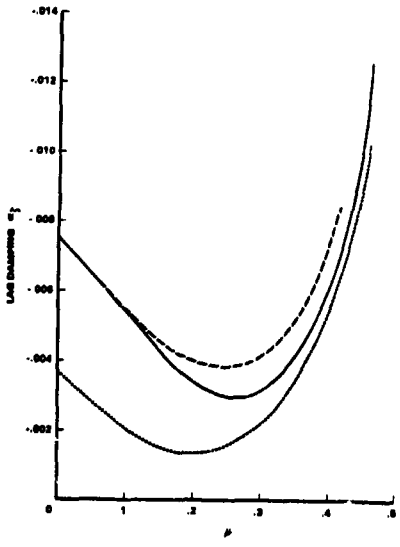

Fig. 7(b) Stiff-lag rotor, $C_w/\sigma=0.2$

Fig. 7 Damping of low frequency cyclic lag mode for different advance ratio μ for a stiff lag rotor (ν =1.15, ν_ζ=1.4, ν_θ=5, R_s=0)

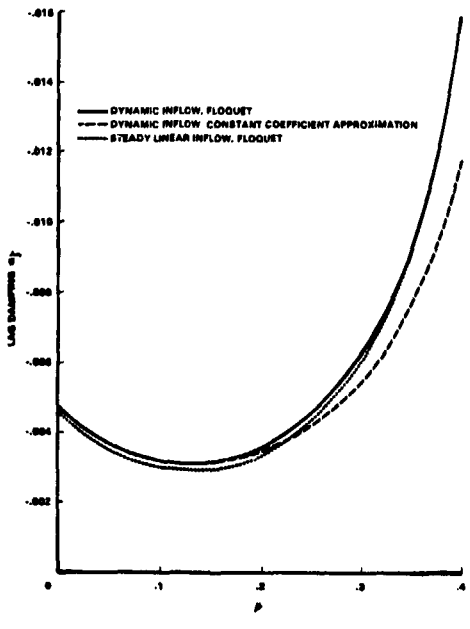

Fig. 8(a) Soft lag rotor, $C_w/\sigma=0.1$

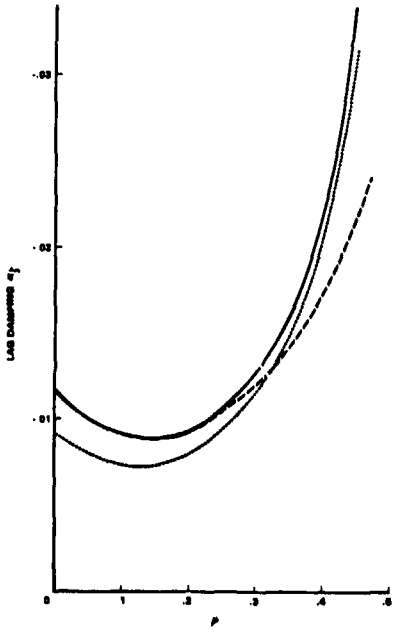

Fig. 8(b) Soft lag rotor, $C_w/\sigma=0.2$

Fig. 8 Damping of low frequency cyclic lag mode for different advance ratios of soft-lag rotor (ν_β=1.5, ν_ζ=0.57, ν_θ=5, R_s=0)

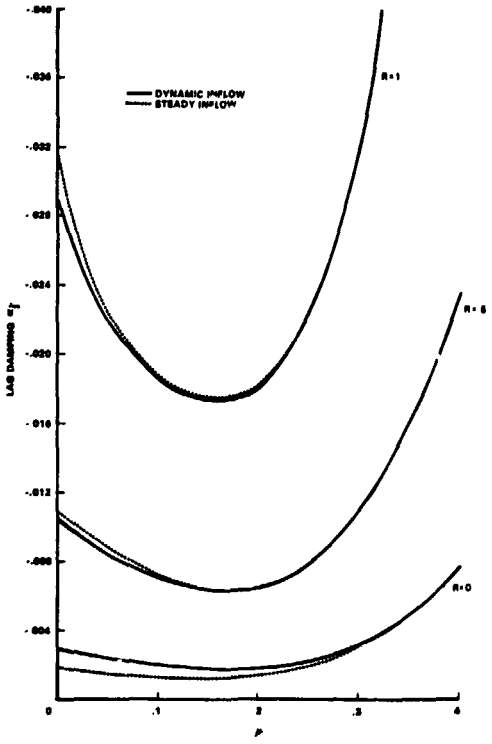

Fig. 9 Effect of structural coupling on low frequency cyclic mode (regressive) for stiff inplane rotor for $C_W/\sigma=.1$ ($\nu_\beta=1.5$, $\nu_\zeta=1.4$, $\nu_\theta=5$)

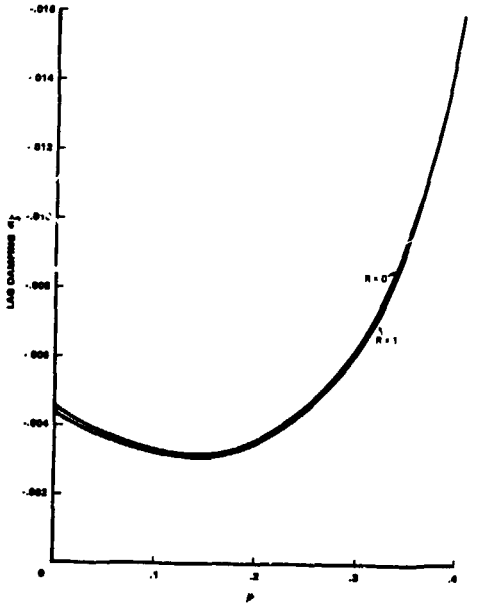

Fig. 10 Effect of structural coupling on low frequency cyclic mode for soft lag rotor ($C_W/\sigma=.1$, $\nu_\beta=1.15$, $\nu_\zeta=0.57$, $\nu_\theta=5$)

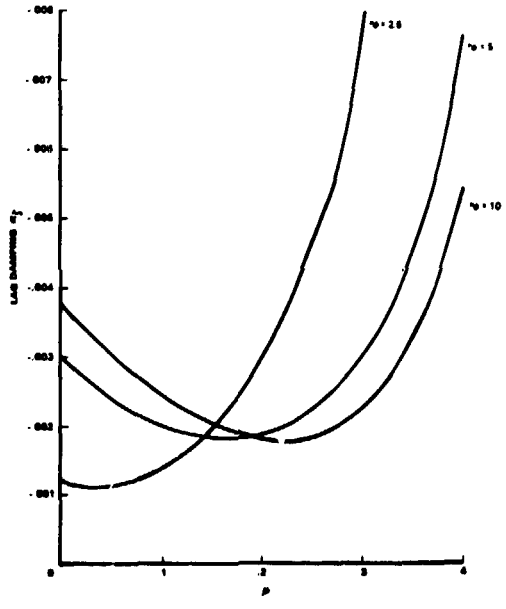

Fig. 11 Effect of torsional stiffness on low frequency cyclic mode for stiff lag rotor ($C_W/\sigma=.1$, $\nu_\beta=1.15$, $\nu_\zeta=1.4$, $R_S=0$, Dynamic Inflow)

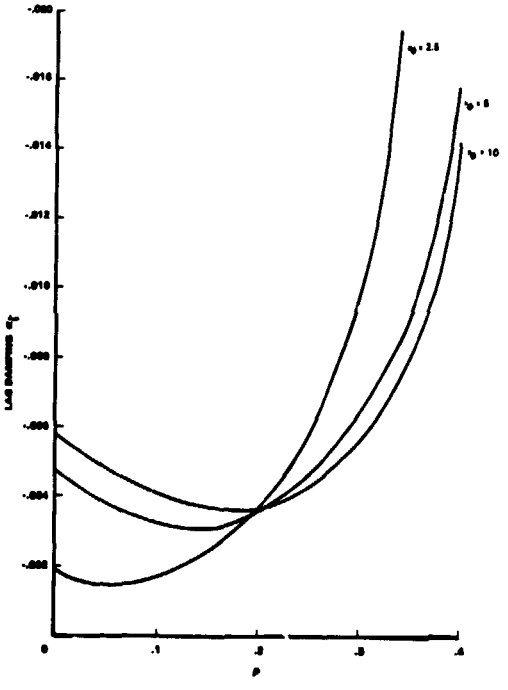

Fig. 12 Effect of torsional stiffness on low frequency cyclic mode for soft lag rotor ($C_W/\sigma=.1$, $\nu_\beta=1.15$, $\nu_\zeta=.57$, $R_S=0$, Dynamic Inflow)

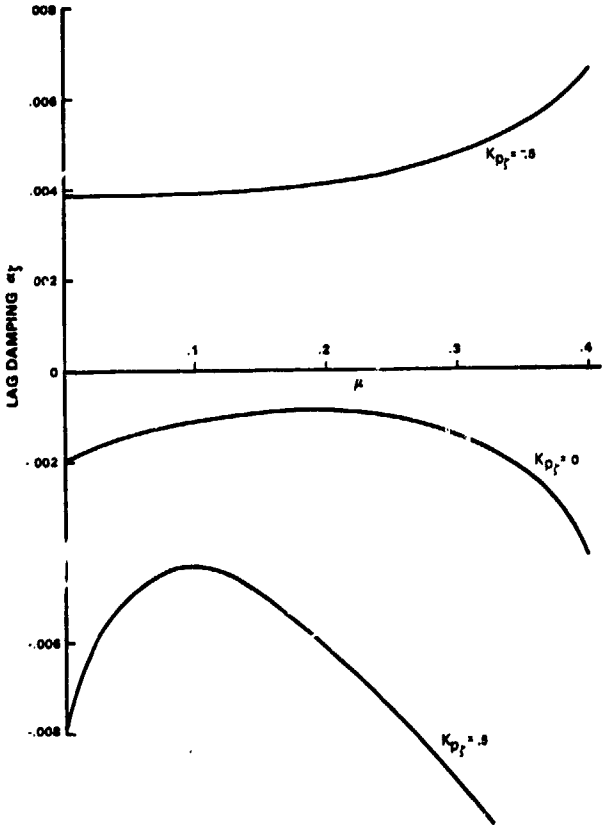

Fig. 13(a) Stiff lag rotor, ν_ζ=1.4

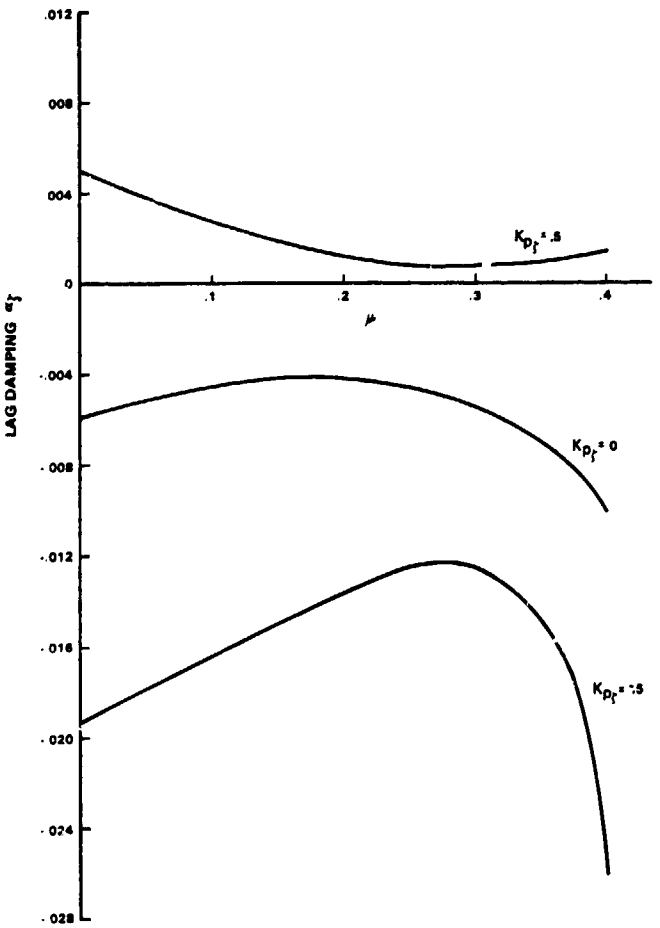

Fig. 13(b) Soft lag rotor, ν_ζ=.57

Fig. 13 Effect of pitch-lag coupling on low frequency cyclic lag mode (C_W/σ=.1, ν_β=1.15, R_S=0, Dynamic Inflow)

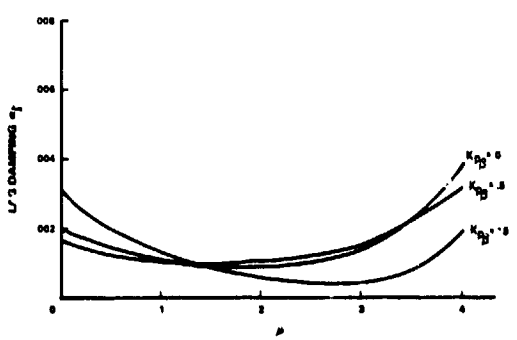

Fig. 14(a) Stiff lag rotor, ν_ζ=1.4

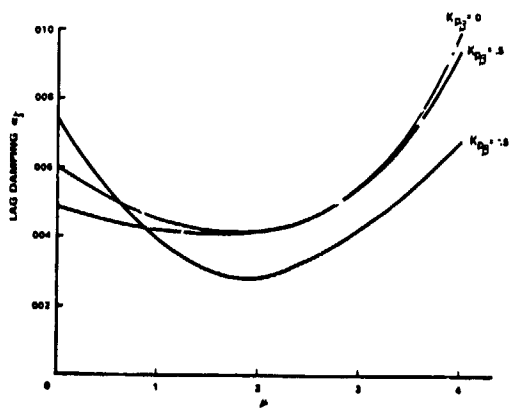

Fig. 14(b) Soft lag rotor, ν_ζ=.57

Fig. 14 Effect of pitch-flap coupling on low frequency cyclic lag mode (C_W/σ=.1, ν_β=1.15, R_S=0, Dynamic Inflow)

DISCUSSION
Paper No. 16

FLAP-LAG-TORSION STABILITY IN FORWARD FLIGHT
Brahmananda Panda
and
Inderjit Chopra

Wayne Johnson, NASA Ames Research Center: Could you describe again the manner in which you trimmed the rotor in forward flight? I noticed in your plot of flapping motion that you had about one degree of 1 per rev flapping motion, so could you tell us how the rotor was trimmed for these results?

Panda: First, we obtained the vehicle trim equations and calculate the control θ_o, θ_{1c}, and θ_{1s}. And using that with the coupled flap-lag-torsion blade equations for solving the trim.

Johnson: Did you trim to zero moment about some center of gravity of a helicopter below the rotor hub, is that what you did?

Panda: Yes.

Peretz Friedmann, University of California, Los Angeles: I wanted to be sure that I understand what kind of model you are using. You have an offset-hinged, spring-restrained blade model with flap, lag, and torsion degrees of freedom, is that correct?

Panda: Yes.

Friedmann: Then I just wanted to comment that at the European Rotorcraft Forum this August a gentleman by the name of Neelakanthan did exactly the same problem. He also did the elastic blade with two flap, two lag, and two torsional degrees of freedom and his results indicated that the model you are using is not safe at all times, so I am just suggesting that maybe you should qualify your conclusions.

Bill Bousman, U.S. Army Aeromechanics Laboratory: I haven't had time to look at these last two papers, but I think that most of the stuff Peretz has done over the years and other people--Dave Peters--has not shown an instability at high speed and there is none shown here in the lag mode. It's just the continuing stabilizing effect as the inflow increases. Dr. Reddy showed Floquet splitting roots and a destabilizing effect and I guess it's an open question [whether] this is something new. Was it just that his torsion [frequency] was 3 per rev or what?

Friedmann: I just wanted to say, Bill, that the instability that Reddy has shown is one which appeared for a stiff inplane case in the paper which Kottapalli and I have written and he just checked it out and he got the same instability.